Physics – Uspekhi **60** (4) 402 – 411 (2017)

FROM THE CURRENT LITERATURE

PACS numbers: 74.20.Mn, 74.25.Dw, **74.72. – h**, **74.70. – b**

Superconducting phase diagrams of cuprates and pnictides as a key to understanding the HTSC mechanism

K V Mitsen, O M Ivanenko

DOI: https://doi.org/10.3367/UFNe.2016.12.038000

Contents

Abstract. This paper reviews experimental phase diagrams of cuprates and pnictides to demonstrate that specific features of the superconducting phase diagrams in both HTSC families can be understood within the framework of the proposed approach, which assumes the formation, under heterovalent doping, of localized trion complexes consisting of a doped carrier and charge transfer (CT) excitons. The geometry of such cells containing CT excitons (CT plaquettes) in the basal plane of the crystal is determined by its crystal structure and the type of dopant, so that the dopant concentration range corresponding to the existence of a percolation cluster of CT plaquettes can be readily determined for each particular compound. These dopant concentration ranges coincide with good accuracy with the experimental ranges of superconducting domes in the phase diagrams of the HTSC compounds considered. The generation of free carriers and the mechanism of superconducting pairing in this pattern is related to biexciton complexes (Heitler–London centers) emerging in neighboring CT plaquettes.

Keywords: superconducting phase diagram, cuprates, pnictides, charge transfer exciton, mechanism of high-T_c superconductivity

1. Introduction

The nature of the normal state and the mechanism of superconductivity in two high-temperature superconducting families — cuprates and pnictides — still remain an issue of animated discussion. Undoped cuprates, as follows from experiment and as is supported by band calculations, possess electronic structures substantially different from those of pnictides. Still, despite the differences in their electronic structures, these compounds demonstrate a number of similar features. Among them, we would like to single out the following:

(1) *Low concentration of charge carriers*. Even at optimal doping, the carrier concentration in cuprates and pnictides is lower than 10^{22} cm^{-3}, which corresponds to an average distance of $r_s > 0.4$ nm between the carriers and exceeds the distance between the anion and cation. This means that the interaction inside the cell is essentially unshielded, which enables the existence of well-defined charge transfer (CT) excitons [1].

(2) *High ionicity of cuprates and pnictides*. This suggests a large contribution of Madelung volume energy E_M to the electronic structure of the basal planes and the possibility of locally changing the electronic structure by doping with localized carriers.

(3) *Similarity of cuprate and pnictide phase diagrams*. As is known, the overwhelming majority of undoped cuprates and pnictides are not superconductors. Superconductivity in them emerges as the result of heterovalent doping, i.e., upon partial substitution of another atom for an atom with higher or lower valency. Thus, the superconducting region in the phase diagrams of these two classes is restricted by a certain concentration interval (x_1, x_2), i.e., only within this doping interval are there conditions for the superconducting mechanism to be activated. The dependence of critical temperature $T_c(x)$ within the interval (x_1, x_2) is, in general, dome-shaped (Fig. 1) with a maximum at x_{opt}.

The region of concentrations in the vicinity of x_{opt} corresponding to the region with maximal T_c is conventionally taken to be the region of optimal doping, whereas the concentration regions on the left- and right-hand sides of the optimal doping region are named, respectively, the underdoping and overdoping regions.

Figure 2 plots experimental superconducting phase diagrams of the most well-investigated HTSCs, cuprates and pnictides. As seen in the figure, concentrations x_1, x_{opt}, and x_2

K V Mitsen, O M Ivanenko Lebedev Physical Institute, Russian Academy of Sciences, Leninskii prosp. 53, 119991 Moscow, Russian Federation
E-mail: mitsen@sci.lebedev.ru

Received 11 November 2016, revised 5 December 2016
Uspekhi Fizicheskikh Nauk **187** (4) 431 – 441 (2017)
DOI: https://doi.org/10.3367/UFNr.2016.12.038000
Translated by O M Ivanenko; edited by A Radzig

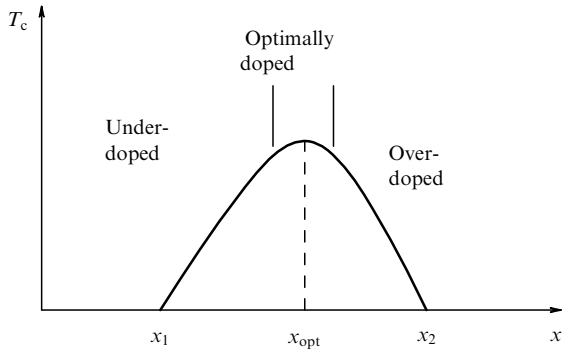

Figure 1. (a) Typical superconducting phase diagram of doped cuprates and pnictides. Superconductivity takes place at a dopant concentration of x within the range of $x_1 < x < x_2$, with the T_c maximum at $x = x_{opt}$.

differ significantly for various HTSCs. Still, the evident similarity among the superconducting phase diagrams for cuprates and pnictides enables the assumption of some common and sufficiently rough mechanism that acts irrespective of the fine details of the band structure and provides the superconducting pairing in these materials.

The aim of this review is to demonstrate that the values of x_1, x_{opt}, and x_2 for various HTSCs can be calculated based on the superconducting pairing mechanism common for cuprates and pnictides. In this regard, in a number of cases, when superconducting phase diagrams demonstrate fine features (narrow dips, jumps, etc.), the positions of these features can be reproduced with unprecedented accuracy.

2. Mechanism of HTSC heterovalent doping

Let us consider the specific features of HTSC materials under heterovalent doping. The heterovalent doping technique is broadly used in semiconductor studies to provide a given concentration of certain-sign carriers in the bulk of a crystal. In semiconductors, the concentration of dopants $N_d \sim 10^{18}-10^{19}$ cm^{-3} is, in most cases, sufficient to achieve a degenerate distribution of carriers at which their concentration and, correspondingly, Hall constant do not depend on temperature. At the same time, cuprates and pnictides, even at optimal doping when the dopant concentration reaches $10^{20}-10^{21}$ cm^{-3}, exhibit a strong dependence of the Hall constant on temperature [10–12] and no direct proportionality of the Hall concentration of carriers to the dopant concentration. What is more, quite a number of experiments exploiting various techniques have obtained convincing proof of the localization of doped carriers in the nearest vicinity of the dopants [13–17]. Thus, the experiments demonstrate that the doped carriers' localization regions do not overlap.

This evidence, if recognized, gives rise to several questions:

(1) What is the mechanism of doped carrier localization?

(2) Where does superconductivity come from and what does the HTSC superconducting phase diagram reflect in this case?

(3) What is the mechanism of free carrier generation?

(4) What is the mechanism of superconductivity?

As an answer to the first question, we consider a mechanism of HTSC heterovalent doping, in which doped carriers are self-localized as the result of the formation of trion complexes. In this complex, a doped carrier is bound by Coulomb interaction with CT excitons that are generated in the vicinity of a given carrier due to a local strain of the electronic structure. The proposed mechanism, as we will show, can (in general) lead to the formation of an inhomogeneous phase whose properties coincide with the experimentally observed properties of HTSCs.

Figures 3a, b display an arrangement of anions and cations (their projections, to be more exact) in the basal planes of cuprates and pnictides. In cuprates, Cu and O ions lie in the same plane, whereas in pnictides, Fe ions reside in the plane and As ions occupy the vertices of regular tetrahedra in such a way that their projections form a square sublattice in the basal plane.

Cuprates in undoped states constitute antiferromagnetic Mott insulators in which the empty subband of copper $3d^{10}$ states is separated from the filled oxygen O2p band by a gap energy $\Delta \sim 2$ eV. In undoped pnictides that are antiferromagnetic (bad) metals, states on the Fermi surface are formed mainly by Fe orbitals, whereas electron states on As lie ~ 2 eV lower than the Fermi energy E_F [18–20]. Thus, *to transfer an electron from an anion* (O, As) *to a cation* (Cu, Fe), *approximately the same energy of* ~ 2 eV *should be spent in both cuprates and pnictides*.

Figures 3c, d give schematically the band structures of (c) undoped cuprates (in electron representation) and (d) undoped pnictides (in hole representation). As follows from the figures, energy Δ_{ib} required for interband transition related to the transfer of an electron from an oxygen ion to a copper ion (in cuprates) (Fig. 3c) or the transfer of a hole from an iron ion to arsenic ion (in pnictides) (Fig. 3d) is in both cases approximately the same: $\Delta_{ib} \sim 2$ eV.

At the same time, exciton-like excitation is also possible, which has a lower energy $\Delta_{ct} < \Delta_{ib}$ and corresponds to the local transfer of an electron (hole) from an anion (cation) to the nearest cation (anion) (Fig. 4a, b) to form the bound state (of a CT exciton).

If Δ_{ib} is somehow gradually decreased, we will first arrive at a state with $\Delta_{ib} = \Delta_{ib}^*$, in which $\Delta_{ct} = 0$ (i.e., $\Delta_{ib}^* \leqslant E_{ex}$, where E_{ex} is the CT exciton binding energy). If Δ_{ib} is decreased homogeneously, the condition $\Delta_{ct} = 0$ will be satisfied for the entire basal plane. If we locally suppress Δ_{ib} in some regions, a continuous cluster of the phase with $\Delta_{ct} = 0$ will emerge at exceeding the percolation threshold over those regions.

Let us consider a phase with $\Delta_{ct} = 0$ (i.e., $\Delta_{ib}^* \leqslant E_{ex}$). This means that two-particle transitions to and from become possible between two single-particle states (L electron + d hole), on the one hand, and an exciton two-particle state (d electron + L hole), on the other hand. For this reason, electron (hole) states in L (d) bands in a phase with $\Delta_{ct} = 0$ should be considered as a superposition of band and exciton states.

The events corresponding to the generation of a CT exciton (localized in a unit cell) involve, in cuprates, the occurrence of an electron on the central Cu cation and a hole distributed over four surrounding anions of O; in pnictides, they involve the occurrence of a hole on the As anion and an electron distributed over four surrounding cations of Fe. This *hydrogen-like ionic complex, for which the condition* $\Delta_{ct} = 0$ *is satisfied and in which a CT exciton, resonantly interacting with the band states, can be formed, will be called a CT plaquette*. In this complex, the state of an electron (in cuprates) and a hole (in pnictides) should be considered as a superposition of band and exciton states.

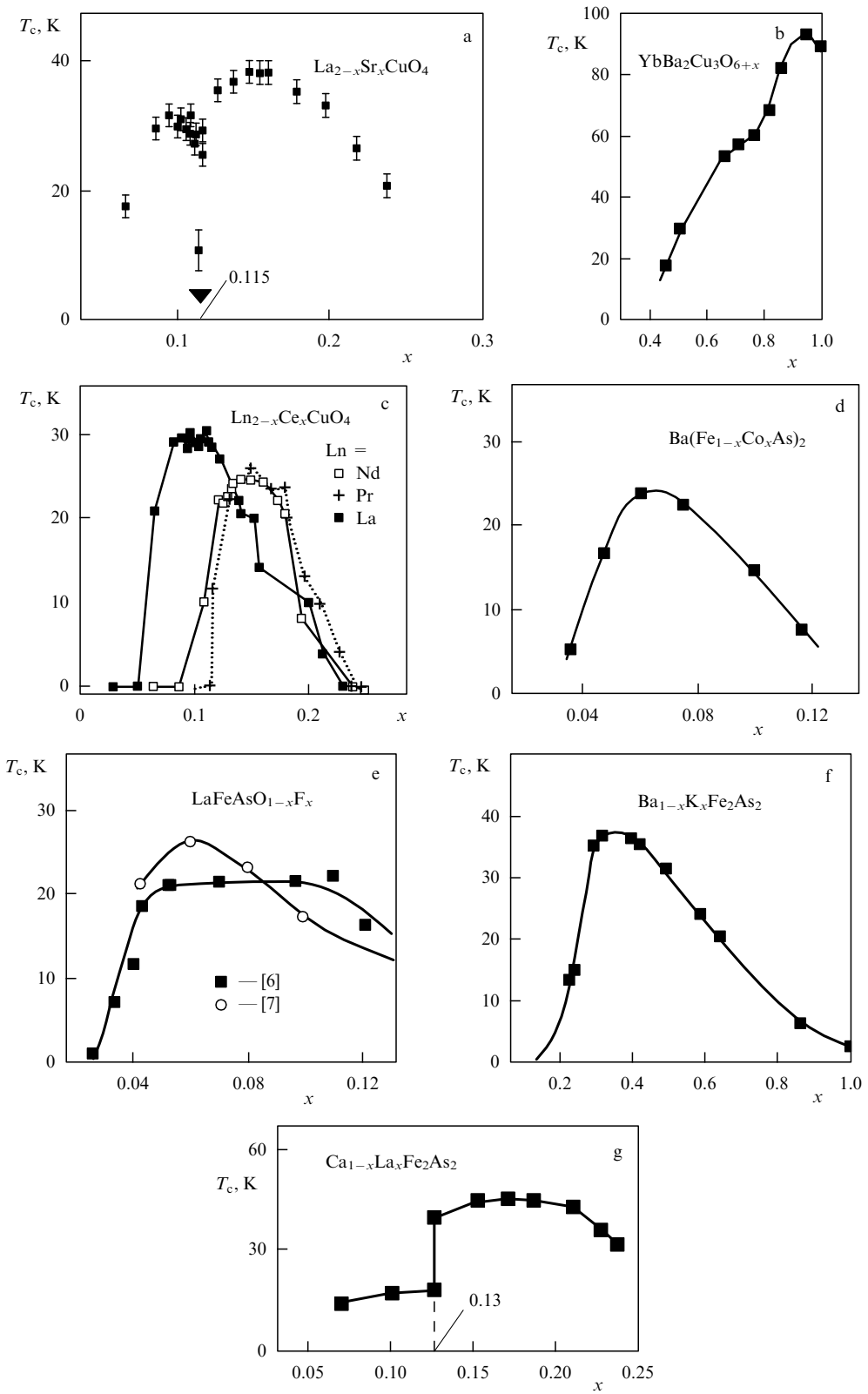

Figure 2. Experimental phase diagrams of some cuprates and pnictides: (a) $La_{2-x}Sr_xCuO_4$ [2]; (b) $YBa_2Cu_3O_{6+x}$ [3]; (c) $Ln_{2-x}Ce_xCuO_4$ [4]; (d) $Ba(Fe_{1-x}Co_xAs)_2$ [5]; (e) $LaFeAsO_{1-x}F_x$ [6, 7]; (f) $Ba_{1-x}K_xFe_2As_2$ [8], and (g) $Ca_{1-x}La_xFe_2As_2$ [9].

Let us consider now how the doping transforms the band structure of parent phases of both cuprates and pnictides (Fig. 5), thus leading to the formation of CT plaquettes.

As the gap energy Δ_{ib} in cuprates and pnictides is largely determined by Madelung energy E_M, we need to locally decrease the value of E_M to form a CT plaquette centered on a given (Cu or As) ion. Hypothetically, this can be done by arranging additional *localized* charges of respective value and sign either on the central (Cu or As) ion or on one of four surrounding ions (of O or Fe), or else in the immediate vicinity between them. Interestingly, exactly this mechanism of decreasing Δ_{ib} appears to be realized in HTSCs under doping.

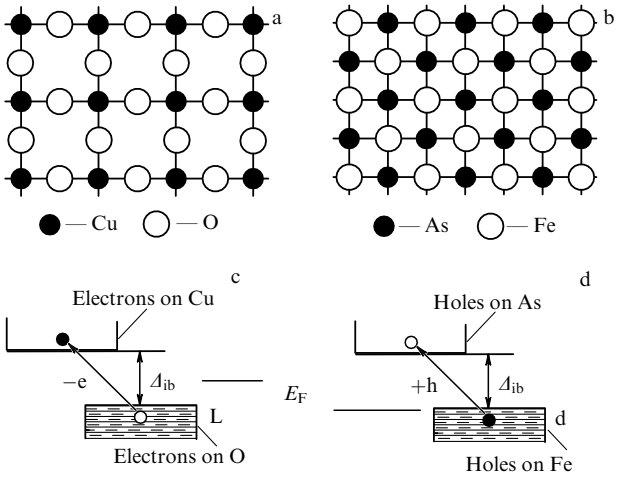

Figure 3. (a, b) Arrangement of the projections of anions and cations in the basal planes of cuprates (a) and pnictides (b); (c) the band structure of undoped cuprates in the electron representation; (d) the band structure of undoped pnictides in the hole representation. Energy Δ_{ib} required for interband transition related to the transfer of an electron from an oxygen ion to a copper ion (in cuprates) or to the transfer of a hole from an iron ion to an arsenic ion (in pnictides) is approximately the same in both cases, equaling ~ 2 eV.

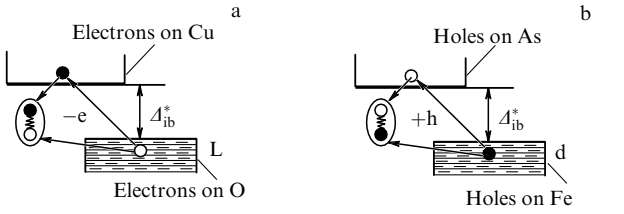

Figure 4. Formation of a CT exciton in cuprates (a) and pnictides (b). To form the CT exciton, the bandgap energy Δ_{ib} should be reduced to $\Delta^*_{ib} < E_{ex}$, where E_{ex} is the CT exciton binding energy.

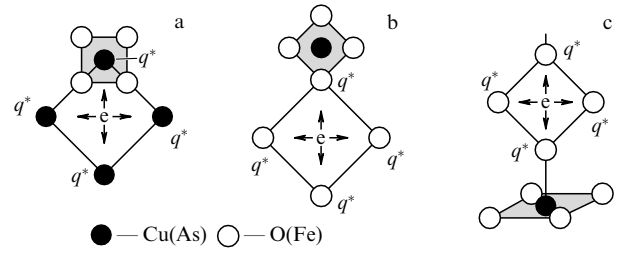

Figure 5. Formation of CT plaquettes and self-localization of doped charges in cuprates and pnictides. The CT plaquette is shaded. (a) Hole doping in pnictides or electron doping in cuprates. (b) Hole doping in cuprates or electron doping in pnictides. (c) A dopant and a doped charge outside the basal plane (YBCO, BSCO, etc.).

Introducing a dopant ion into the lattice is accompanied with the emergence (*in the vicinity of the dopant projection*) *of an additional carrier* (*an electron or a hole*) *in or outside the basal plane*. This doped carrier, in accordance with the neighborhood symmetry, imparts fractional charge $q^* \approx |e|/4$ to corresponding orbitals of each of the nearest ions. In hole doping, holes are distributed over the four nearest ions of O or As, and electrons, in electron doping, over the four nearest ions of Cu or Fe.

Charge q^* emerging on each of four Cu (As) ions (Fig. 5a) locally decreases the Madelung energy. Thus, we neglect the effect of the charge of the dopant, which is at a larger distance. A local decrease in the Madelung energy, in turn, reduces the gap energy Δ_{ib} for the transfer of an electron (hole) to each of the four ions of Cu (As) from the surrounding ions of O (Fe). As estimates imply [21], this decrease is ~ 1 eV at $q^* \approx |e|/4$ and the existing interatomic distances, and, by our assumption, it is sufficient to fulfill the condition $\Delta_{ct} = 0$, i.e., to form CT plaquettes on these ionic complexes.

As each CT plaquette is bound by Coulomb attraction with doped charge q^*, the doped carrier self-localizes in the nearest vicinity of the dopant, which is supported by the results of Refs [13–17].

Thus, the localization boundary of the doped carrier is determined by the condition that the same charge $q^* \approx |e|/4$ sufficient for CT plaquette formation be at this boundary per anion (cation). In fact, a trion complex forms in the basal plane, where the doped carrier is coupled to CT excitons that resonantly interact with the band states. This mechanism of CT plaquette formation (Fig. 5a) is realized in electron-doped cuprates and hole-doped pnictides.

In the case shown in Fig. 5b, doped charge q^* occurring at each of four O (Fe) ions locally decreases the Madelung energy and forms a CT plaquette in the next ion square centered on the nearest Cu (As) ion, because only these ions can be CT-plaquette centers. This scheme is realized for hole-doped cuprates and electron-doped pnictides.

Figures 5a, b illustrate cases where a doped carrier resides in the basal plane. However, it is possible that doped charge q^* localizes outside the plane (Fig. 5c), e.g., on apical ions of oxygen, as it takes place in YBCO and other two-plane cuprates. This charge also decreases the electron energy on the nearest Cu ion by the required value and thereby forms a CT plaquette in the CuO_2 plane.

If the dopant concentration is increased in the cases shown in Figs 5a, b until the neighboring trion complexes begin to overlap each other, this will lead to the delocalization of doped carriers and, correspondingly, to a transition to the overdoped phase. In the case of Fig. 5c, transition to the overdoped phase with the doping level increasing will occur when the calculated charge q^* per apical cation will significantly exceed the required value of $|q^*| \sim |e|/4$. This takes place, in particular, in the HTSC $Ba_2Sr_2CaCu_2O_{8+x}$ ($0 < x < 2$), where higher doping levels can be achieved than with $YBa_2Cu_3O_{6+x}$ ($0 < x < 1$).

According to the above said, CT plaquettes limiting the propagation of the doped carrier are formed around the dopant projection in the basal plane. In the case shown in Fig. 5c, when the doped carrier is localized outside the basal plane, two CT plaquettes are formed, one in each plane; at the same time, the number of CT plaquettes formed around the doped carrier localization region depends in the cases shown in Figs 5a, b on the neighborhood symmetry and, as will be seen further on, can vary from 4 up to 8.

Thus, isolated localization regions of doped carriers enclosed by CT plaquettes are formed in the basal plane of doped HTSCs at sufficiently low dopant concentrations. If we accept this pattern, a question arises: what do the superconducting phase diagram of an HTSC and its dome-like shape reflect? Because $0 < x_{opt} < 1$, i.e., the superconducting phase exists generally in an intermediate dopant concentration range, then the only possibility of explaining the position of the dome and its shape within the framework of the model built is to relate the superconducting phase with the CT plaquette phase — that is, to assume that superconductivity

takes place in the percolation cluster that unites the CT plaquettes. A plaquette cluster should be considered as a continuous network of adjacent cations (in cuprates) or anions (in pnictides) that are the centers of CT plaquettes. A CT-phase cluster can consist of two or more CT plaquettes (see Sections 3 and 4 below). As a variant of such a cluster, we will also consider a plaquette network where small plaquette clusters that comprise two or more CT plaquettes are linked by regions of doped carrier localization.

Further, we will determine the existence regions of percolation clusters composed from CT plaquettes in the basal planes of various HTSC compounds and will compare them with the concentration ranges of dopants corresponding to the existence of high-temperature superconductivity in the phase diagrams of those compounds.

When a doped charge resides in the basal plane, for the percolation network of CT plaquettes to be formed, it is necessary that the dopant projections be at some *fixed* distances l_D from each other forming clusters of CT plaquettes (Fig. 6). The percolation network in the basal plane can be formed if the dopant projections are ordered into a square superlattice with parameter l_D. For this reason, a large role in the formation of the superconducting phase is played by dopant ordering, which provides the possibility of forming percolation clusters of CT plaquettes. We believe that, in doped cuprates and pnictides, there is a 3D ordering of localized carriers (projections of dopants) into 3D lattices with parameter l_D determined by the dopant concentration (with site occupation $v < 1$). This ordering, in our opinion, is due to the emergence of elastic strains in the presence of various sizes of dopant and matrix atoms and/or due to the orientational interaction of dipoles (dopant ion + localized doped carrier) [22]. In the formed superlattice, the dopant projections are assumed to be randomly distributed (in any event, it occurs near and above the percolation threshold).

Let us have a domain in which the dopant projections are randomly distributed over the nodes of a superlattice with parameter l_D. The dopant concentration $x_{max} = 1/l_D^2$, corresponding to the full filling of lattice nodes, will be taken for the upper boundary of the optimal doping region. This boundary fitting the maximal concentration of CT plaquettes also corresponds, according to our assumption, to the maximum T_c. For the lower boundary, $x_{min} = 0.593/l_D^2 \approx 0.6/l_D^2$, we will conventionally take a dopant concentration corresponding to the site percolation threshold on a square lattice with parameter l_D [23]. This choice is caused by the fact that the existence of physically significant domains with a percolation network of dopant projections, spaced by a distance of l_D from each other, is only possible for

$$\frac{0.6}{l_D^2} < x < \frac{1}{l_D^2}\,.$$

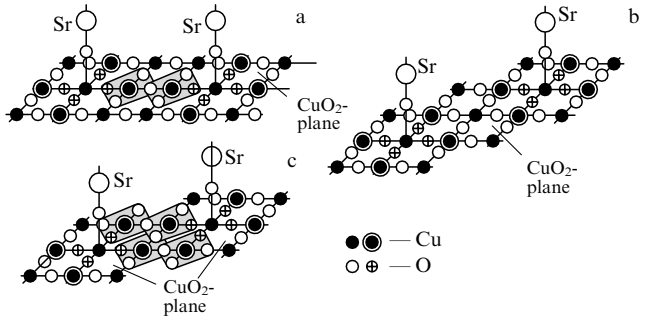

Figure 7. Formation of the percolation network of CT plaquettes (shaded) in $La_{2-x}Sr_xCuO_4$ at various distances between dopant projections: (a) $l_D = 3a$; (b) $l_D = a\sqrt{8}$, and (c) $l_D = a\sqrt{5}$. Dots inside a ring mark Cu ions, which are the centers of CT plaquettes.

This does not mean that the percolation cluster on a lattice with parameter l_D should occupy the entire crystal, but only that such domains will exist within only this concentration range. In this regard, superconductivity in the entire crystal can emerge owing to the Josephson coupling between such domains. The particular shape of the $T_c(x)$ curve is determined by the possibility of realizing various types of dopant ordering in this crystal structure [24, 25].

We now move to a consideration of particular compounds.

2.1 $La_{2-x}Sr_xCuO_4$

In the case of the $La_{2-x}Sr_xCuO_4$ compound, the doped hole emerging at the substitution of Sr^{2+} for La^{3+} resides in the CuO_2 plane (Fig. 7) and is distributed over four oxygen ions pertaining to the oxygen octahedron adjacent to the Sr ion [13, 14]. Each of the four fractional charges q^* on oxygen ions forms a CT plaquette in the next ion square centered on the nearest Cu cation (Fig. 5b). It is readily seen that only two variants of the relative arrangement of two nearest projections of Sr on the CuO_2 plane are possible, so that they could form a pair of neighboring CT plaquettes (Figs 7a and 7c). These cases correspond to two possible separations between them, $l_D = 3a$ and $l_D = a\sqrt{5}$ (a is a lattice parameter). The pairs of CT plaquettes formed in the CuO_2 plane centered on Cu ions (dots inside a ring) are encircled with solid lines. Notice that in an intermediate case, when the distance

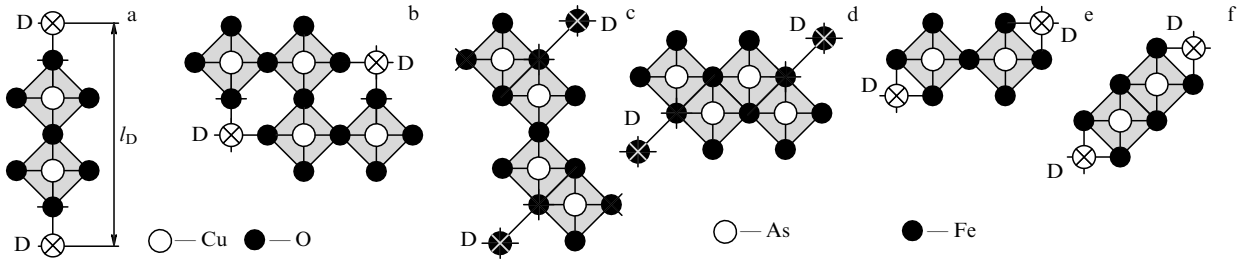

Figure 6. Examples of the arrangement of dopant (D) projections in the basal plane that lead to the formation of a chain of CT plaquettes (shaded) composing percolation clusters: (a, b) cuprates (doped with holes or electrons); (c–f) pnictides (doped with electrons (c, d) or with holes (e, f)).

between the Sr projections is $l_D = a\sqrt{8}$ (Fig. 7b), no pairs of CT plaquettes are formed on neighboring Cu ions.

In accordance with two different variants of dopant projection arrangement, the $La_{2-x}Sr_xCuO_4$ phase diagram is expected to have two regions of optimal doping for $0.066 < x < 0.11$ and for $0.12 < x < 0.2$ (corresponding to the ordered arrangement of Sr projections onto 3×3 and $\sqrt{5} \times \sqrt{5}$ lattices). It should be noted that the experimental value of the upper optimal concentration, $x = 0.15$ (optimal in the sense of the maximum magnitude of T_c), differs from the expected value, $x = 1/5$, though a jumplike decrease in the volume of the superconducting phase is observed namely at $x = 1/5$ [26]. This discrepancy can be explained by the onset of formation of normal metal clusters, which begins for $x > 0.15$ [27]. Within the interval of $0.11 < x < 0.12$, domains with the percolation network of CT plaquettes cannot exist. This is the so-called 1/8 anomaly, which, however, takes place not at $x = 0.125$ but, according to this consideration, at $x = 0.115$, in total agreement with experimental data (Fig. 2a) [2, 28].

2.2 $Ln_{2-x}Ce_xCuO_4$

In the electron-doped HTSC $Ln_{2-x}Ce_xCuO_4$, the doped electron emerging upon substituting Ce^{4+} for Ln^{3+} is in the CuO_2 plane (Fig. 8) and is distributed over four Cu ions. In accordance with Fig. 5a, four external ions of Cu are the centers of CT plaquettes. Similar to $La_{2-x}Sr_xCuO_4$, two types of arrangements of dopant projections and, respectively, two regions of optimal doping — $0.066 < x < 0.11$ and $0.12 < x < 0.2$ — where a network of CT plaquettes can be formed, are possible in this compound. However, in the phase diagrams of $Nd_{2-x}Ce_xCuO_4$ and $Pr_{2-x}Ce_xCuO_4$, only one superconducting dome is observed with a T_c maximum at $x = 0.15$ and falling to zero when increasing $x \to 0.2$. We associate this discrepancy with a low degree of ordering of Ce ions in the lattice owing to the proximity of the atomic radii of Nd, Pr, and Ce ($r_{Nd} \approx r_{Pr} \approx r_{Ce} \approx 0.185$ nm [29]). At the same time, in the phase diagram of $La_{2-x}Ce_xCuO_4$ ($r_{La} \approx 0.195$ nm [29]), two superconducting domes can clearly be seen in the expected intervals with the local T_c maxima at $x = 0.11$ and $x = 0.15$, as in $La_{2-x}Sr_xCuO_4$ (Fig. 2c [4]).

2.3 $YBa_2Cu_3O_{6+\delta}$

The parent compound $YBa_2Cu_3O_6$ is doped by introducing excess oxygen (δ) into the plane of the chains. When two positions in succession in the chain are occupied by oxygen ions (Fig. 9), an oxygen square forms, with one hole distributed over four oxygen ions of this square (circles with 'plus' symbols). Thus, additional positive charges $q^* \approx |e|/4$ emerge on the apical oxygen ions nearest to the in-plane Cu ions (double circles), which results in the formation of CT plaquettes with the center on these Cu ions (Fig. 5c). As the concentration of oxygen pairs in a chain is equal to x^2, the percolation cluster of the CT-plaquette phase will exist for $x^2 > 0.593$, i.e., for $x > 0.77$. Thus, the region of optimal doping for $YBa_2Cu_3O_{6+\delta}$ falls within the interval of $0.77 < \delta < 1$, in accordance with experiment (Fig. 2b [3]). We should note that YBCO is the only case known to us where doping can realize the condition $\Delta_{ct} = 0$ for the entire basal plane. In the case, for example, of another double-plane cuprate $Ba_2Sr_2CaCu_2O_{8+x}$, where $0 < x < 2$, inhomogeneous filling of excess oxygen positions leads to various charges q^* on the apical ions of oxygen, a consequence of which is the co-existence of underdoped and overdoped regions in one basal plane, along with optimally doped regions.

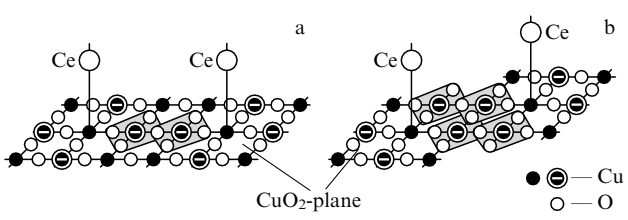

Figure 8. Formation of CT plaquettes (shaded) in $Ln_{2-x}Ce_xCuO_4$ at various distances between dopant projections: (a) $l_D = 3a$; (b) $l_D = a\sqrt{5}$; double circles mark Cu ions, which are the centers of CT plaquettes. Clusters of CT plaquettes are shaded.

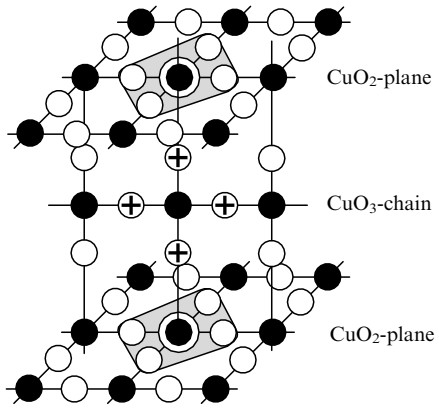

Figure 9. Formation of CT plaquettes in $YBa_2Cu_3O_{6+\delta}$. Provided that two positions in succession in the chains are filled with oxygen ions, one hole distributed over four ions of the oxygen square emerges in this square. Thus, charge $q^* \approx |e|/4$ is imparted to the apical oxygen ions nearest to the Cu ion. This is sufficient to form a CT plaquette in each CuO_2 plane (CT plaquettes are shaded).

2.4 $Ba(Fe_{1-x}Co_xAs)_2$

In this compound, doping is performed by substituting Co atoms for Fe in the basal plane (Fig. 10). An additional electron emerging at the substitution imparts charge $q^* \approx -|e|/4$ to each of four surrounding Fe ions (Fig. 10a). In principle, two variants of combining CT plaquettes into a continuous cluster (Figs 10b, c) are possible; they differ by the different arrangements of Co ion projections at the same distance between As anions. In an ordered arrangement of dopants in a $\sqrt{20} \times \sqrt{20}$ lattice, we have a percolation network of CT plaquettes (Fig. 10b). A corresponding concentration of optimal doping is $x = 0.05$, while the concentration corresponding to the percolation threshold is $x = 0.03$, which is in good agreement with the experimental phase diagram of $Ba(Fe_{1-x}Co_xAs)_2$ (Fig. 2d). It is readily seen that other distances between dopants ensuring the formation of a percolation cluster of CT plaquettes are possible within the interval of $a\sqrt{13} \leqslant l_D \leqslant a\sqrt{20}$, too (Fig. 10e). This interval corresponds to the concentration range of $0.03 \leqslant x \leqslant 0.08$ (Fig. 2d [5]).

2.5 $LaFeAsO_{1-x}F_x$

In this compound, one electron is doped into the basal plane upon substituting fluorine for oxygen. The projection of the F

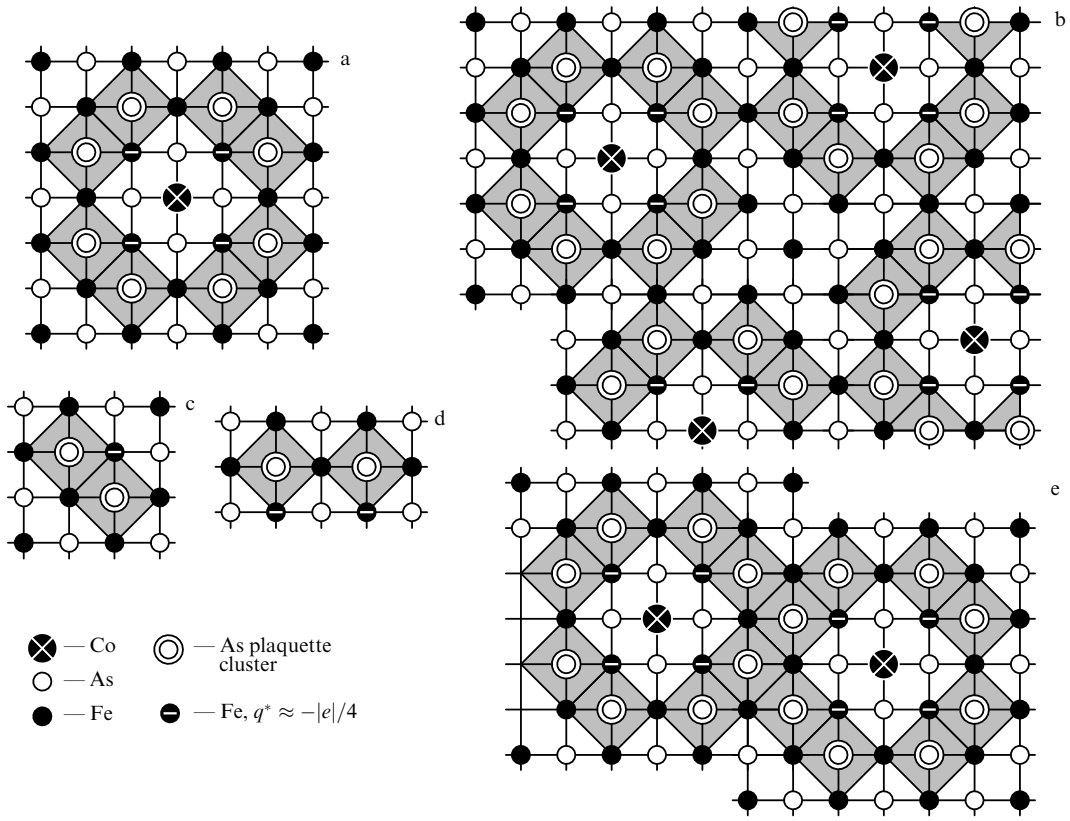

Figure 10. Formation of a cluster of CT plaquettes in $Ba(Fe_{1-x}Co_xAs)_2$. White dots indicate projections of As ions at the vertices of tetrahedra onto the Fe plane; (a) formation of CT plaquettes (shaded) around the Co ion; (c, d) possible variants of combining CT plaquettes into a continuous cluster; the variants differ by different arrangements of Co ion projections at the same distance between As anions; (b, e) formation of a percolation cluster of CT plaquettes on $\sqrt{20} \times \sqrt{20}$ and $\sqrt{13} \times \sqrt{13}$ square lattices.

ion onto the basal plane coincides with the position of the Co ion in Fig. 10a. As a consequence, the symmetry of doped charge distribution in $LaFeAsO_{1-x}F_x$ will be similar to that in $Ba(Fe_{1-x}Co_xAs)_2$ (Fig. 10a). Therefore, the phase diagrams of $LaFeAsO_{1-x}F_x$ and $Ba(Fe_{1-x}Co_xAs)_2$ should coincide in respective concentration ranges, which is consistent with experiment (Fig. 2e [6, 7]).

At the same time, a comparison of the electron phase diagrams for $LaFeAsO_{1-x}F_x$ and other '1111' compounds ($SmFeAsO_{1-x}F_x$ and $CeFeAsO_{1-x}F_x$) [30] demonstrates significant discrepancies in the positions of the superconducting domes. These discrepancies, as shown in paper [31], appear to be due to a difference in the real content of fluorine in specimens of $SmFeAsO_{1-x}F_x$ and $CeFeAsO_{1-x}F_x$ from the nominal content determined by the initial weight. At the same time, the real content of fluorine in $LaFeAsO_{1-x}F_x$ coincides with the nominal value. With respective corrections made, the regions of the superconducting domes in the phase diagrams of '1111' compounds will coincide [31].

2.6 $Ba_{1-x}K_xFe_2As_2$

Consider now the hole-doped compound $Ba_{1-x}K_xFe_2As_2$. Substitution of K for Ba leads to emerging in one of the two FeAs planes a hole that is distributed over the four nearest As ions (Fig. 11a), imparting to them charge q^*. (Localization of the doped holes on As ions is indirectly confirmed by the results of paper [32], where the contribution of electron carriers to thermal conductivity was observed in the $Ba_{1-x}K_xFe_2As_2$ compound up to $x = 0.88$.) Thus, four CT plaquettes are formed around each projection of a K ion.

A percolation cluster of CT plaquettes can be produced at an ordered arrangement of dopants into a $\sqrt{10} \times \sqrt{10}$ lattice (Fig. 11b). The potassium concentration conforming to the total filling of the $\sqrt{10} \times \sqrt{10}$ lattice is $x = 0.2$ (with account for the fact that only each second K ion dopes a hole to a given FeAs plane), and the appropriate concentration conforming to the percolation threshold is $x = 0.12$. The optimal arrangement is the ordering of dopant projections into a $\sqrt{5} \times \sqrt{5}$ lattice (Fig. 11c), which corresponds to an optimal dopant concentration $x = 0.4$. The concentration values determined in this way are quite consistent with the phase diagram of $Ba_{1-x}K_xFe_2As_2$ (Fig. 2f [8]).

2.7 $Ca_{1-x}La_xFe_2As_2$

In this compound, substituting La for Ca leads to the emergence of an additional electron in one of the two FeAs planes, which imparts charge $q^* \approx -|e|/4$ to each of four Fe ions nearest to the projection of La (Fig. 12). As a result, eight CT plaquettes form around these Fe ions.

The maximal distance between dopant projections, required to form a percolation cluster of CT plaquettes, is $l_D = \sqrt{18}$ (Fig. 12c). The percolation threshold upon ordering dopant projections into a $\sqrt{18} \times \sqrt{18}$ superlattice corresponds to a concentration of $x = 0.067$ (with account for the fact that only each second La ion dopes an electron to the FeAs plane).

Optimal doping, as seen in Fig. 12b, is in correspondence with the complete ordering of dopant projections into the 3×3 superlattice. A concentration corresponding to an optimal doping is $x = 0.22$; respectively, a concentration

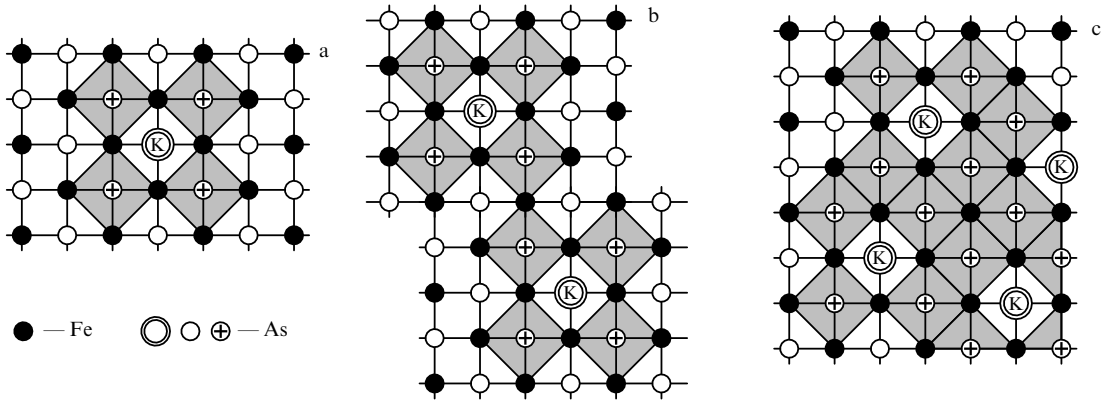

Figure 11. (a) Formation of CT plaquettes in $Ba_{1-x}K_xFe_2As_2$. White dots label projections of As ions at the vertices of tetrahedra onto the Fe plane; a double circled 'K' symbol is the projection of an As ion coinciding with the projection of a K ion onto the Fe plane, and circled 'plus' symbols mark As ions carrying charge q^* and representing the center of a CT plaquette (shaded). (b, c) Formation of a percolation cluster of CT plaquettes on $\sqrt{10} \times \sqrt{10}$ and $\sqrt{5} \times \sqrt{5}$ square lattices.

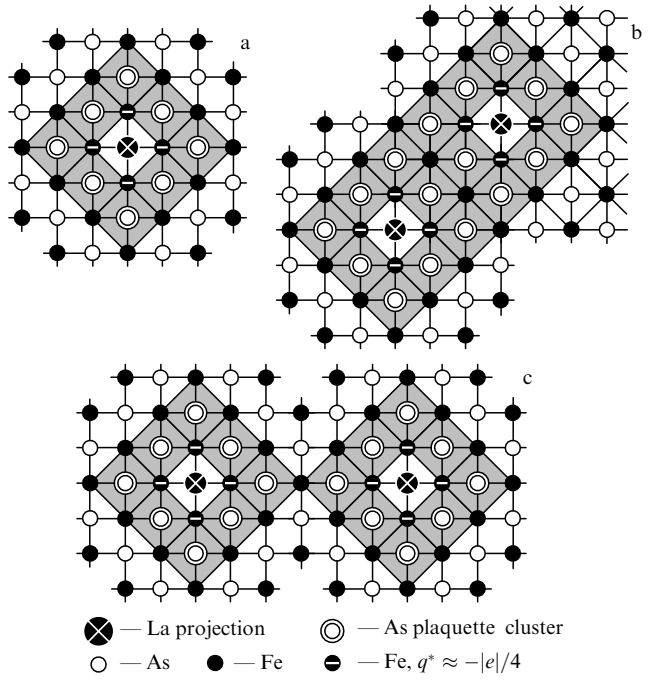

Figure 12. (a) Formation of CT plaquettes in $Ca_{1-x}La_xFe_2As_2$. Eight CT plaquettes (shaded) form around an La projection in one of the FeAs planes; white dots identify As; black dots, Fe; black dots with 'minus' sign, Fe ions with charge $q^* = -|e|/4$. (b) Formation of a percolation cluster of CT plaquettes on a 3×3 superlattice; (c) formation of a percolation cluster of CT plaquettes on a $\sqrt{18} \times \sqrt{18}$ superlattice.

that conforms to the percolation threshold on this lattice is $x = 0.132$. All three concentration values (0.067, 0.13, and 0.22) coincide with the boundaries for the low- and high-temperature superconductivity regions in the experimental phase diagram of $Ca_{1-x}La_xFe_2As_2$ (Fig. 2g [9]).

Thus, we have shown that the regions of concentrations corresponding to the superconducting dome in the phase diagrams of cuprates and pnictides coincide with those of the formation of a percolation cluster of the CT phase.[1] The demonstrated coincidence can serve as an indication of an improper approach that considers cuprates and pnictides to be spatially homogeneous systems with concentrations of carriers determined by the doping level. The fact that the proposed method of constructing phase diagrams proved similarly successful both for cuprates and pnictides is a serious argument in favor of the common nature of the superconducting state in these classes of HTSCs.

It should be emphasized that in the CT phase an electron and hole are bound to reside simultaneously in each of the CT plaquette. It is a hole on the central Cu ion and an electron on the surrounding O ion or an electron on the Cu ion and a hole on the surrounding O ions in the case of cuprates. Whereas in the case of pnictides it is, respectively, an electron on the central As ion and a hole on the surrounding Fe ions or a hole on the As ion and an electron distributed over surrounding Fe ions. Therefore, at first glance it would seem that the electron transfer in such a system is impossible, because the two-electron states in a CT plaquette (in cuprates) or the two-hole state (in pnictides) possess a more high energy, i.e., all carriers are bound here and noncoherent transport in the system turns out to be suppressed. Nonetheless, we will show below that a specific mechanism of free carrier generation evolves in the system considered.

3. Heitler–London centers and generation of free carriers

Let us return to a consideration of the properties of the phase with $\Delta_{ct} = 0$, where a CT plaquette is formed on each cation (in cuprates) or anion (in pnictides). Let there be two CT plaquettes centered on the nearest Cu cations (in cuprates) or As anions (in pnictides). Such a pair of plaquettes forms a Heitler–London (HL) center, which can be considered a solid state analog of the hydrogen molecule [21]. In this center, two electrons and two holes can form a bound state (biexciton) that is energetically lower than the energy of two CT excitons due to the possibility of two holes (electrons) in the singlet state being in the space between the central ions and being attracted simultaneously to two electrons (holes) occurring on these ions. An additional decrease in energy, ΔE_{HL}, can in this case be assessed from the relation $\Delta E_{HL} \sim \Delta E_{H_2}/\varepsilon_\infty^2 \approx 0.2$ eV, where $\Delta E_{H_2} = 4.75$ eV is the binding energy in the H_2 molecule, and $\varepsilon_\infty \approx 4.5-5$ (for cuprates)

[1] Notice that the consideration of the case of HTSCs with heterovalent doping does not rule out the possible existence of compounds where the percolation cluster of CT plaquettes already exists in the undoped phase (e.g., LiFeAs) or forms during isovalent substitution, if the dopant locally decreases Δ_{ib} and becomes a center of a CT plaquette (e.g., $BaFe_2(As_{1-x}P_x)_2$).

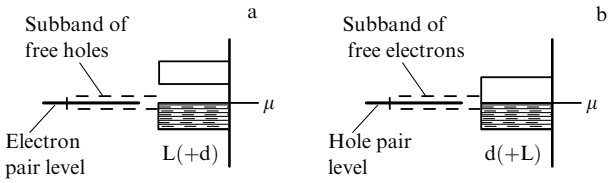

Figure 13. Single-electron band structure diagrams of (a) cuprates (in electron representation) and (b) pnictides (in hole representation); μ is the chemical potential level. The electron (hole) states in the L band (d band) represent a superposition of the band and exciton states. The hole (electron) subband of HL centers is formed for $T > 0$ as a result of their filling with electrons (holes).

[33]. An HL center is considered to be occupied if both electron (hole) states on the central cations of Cu (anions of As) are occupied.

Thus, two electrons on Cu cations (two holes on As anions) will have a lower energy in a CT phase, if they occupy adjacent cations (anions) and two holes (two electrons) bound to them are on the surrounding O anions (Fe cations). These pairs of electrons (holes) occupy a common pair level of HL centers that belong to one percolation cluster (Fig. 13). In this figure, the states of electrons in band L (in cuprates) or holes in band d (in pnictides) represent a superposition of band and exciton states.

When the temperature increases, the biexciton can become ionized without being separated into two excitons. By analogy with the hydrogen molecule, apart from the H_2^+ molecular ion, there is also the bound state of two protons and one electron, namely the Hion. In our case, this corresponds to an ionized HL center, in which two electrons and one hole (in cuprates) or two holes and one electron (in pnictides) form a bound state. The emerging 'spare' hole (in cuprates) or electron (in pnictides) can pass from node to node, thus overlapping the corresponding orbitals of HL centers and forming a hole (electron) subband with the corresponding type of superconductivity at the level of chemical potential μ (Fig. 13).

The concentration of free carriers in the emerging subband of HL centers (holes in cuprates, and electrons in pnictides) will be determined by HL-center occupancy, i.e., by the balance between the rates of transfer of electron (hole) pairs to HL centers and the rates of their departure to the band as a result of the breakdown of a pair state. The value of pair hybridization Γ (or the inverse lifetime of a pair state) depends on temperature [34, 35]:

$$\Gamma \approx kT\left(\frac{V}{E_F}\right)^2$$

(here, V is the single-particle hybridization constant, E_F is the Fermi energy, and T is the temperature). The rate of pair level–band transitions is $\propto \eta\Gamma$. The inverse process (occupancy of a pair level) is determined by the rate of electron–electron scattering; this rate equals $\propto (1-\eta)\,T^2$. Hence, for the occupancy of an HL center, η, we have

$$\eta = \frac{2T}{(T+T_0)}\,,$$

where T_0 is a temperature-independent constant. Correspondingly, one finds for the concentration of additional carriers the following expression: $n = 2NT/(T+T_0)$, where N is the concentration of HL centers. From this relation, it follows that at $T = 0$ the concentration of additional free carriers $n = 0$. (Here, we assume that at $T = 0$ the occupancy of HL centers is negligibly small.) The maximally possible concentration of additional carriers is achieved upon the total filling of HL centers, i.e., if a CT plaquette cluster fills the entire basal plane, then this concentration will equal the concentration of Cu (As) ions in the basal planes. Thus, for $YBa_2Cu_3O_7$ compounds, which have no free carriers at $T = 0$, $n \to 2$ (u-cell)$^{-1}$ as $T \to \infty$, which matches the experimental results [10, 36].

According to the above consideration, noncoherent transport in the normal state occurs due to carriers that emerge upon filling HL centers. However, at $T = 0$ the pair level is not filled, and the concentration of carriers is $n = 0$. Consequently, at $T = 0$ noncoherent transfer would be impossible in view of the absence of free carriers. At the same time, in such a system, where there are an electron and a hole in each CT plaquette (i.e., there are free states to which electrons can pass), coherent transport becomes possible when all carriers of a like sign move in a given direction coherently, as a whole (e.g., superconducting condensate). The latter is possible in the presence of pairing interaction.

As shown in Refs [34, 35, 37–41], accounting for scattering processes with intermediate bound states lying in the vicinity of E_F can lead to a strong renormalization of efficient electron–electron interaction capable of providing high T_c in the system. In a pattern based on the formation of local CT excitons and HL centers, electron–electron attraction emerges due to the formation of a bound state of two electrons (holes) getting at the central cations (anions) of an unfilled HL center and two holes (electrons), emerging with *necessity* on the surrounding ions in the phase with $\Delta_{ct} = 0$. Thus, the basal planes of doped cuprates and pnictides can be considered as one more type of structures (in addition to one-dimensional Little chains [42] and Ginzburg sandwiches [43]) where the exciton mechanism of superconductivity could be realized.

4. Conclusion

This article reviews experimental phase diagrams of cuprates and pnictides to demonstrate that specific features of the superconducting phase diagrams in both HTSC families can be understood within the framework of the approach that assumes the localization of doped carriers in the vicinity of dopants as a consequence of their forming the localized trion complexes consisting of a doped carrier and its surrounding charge transfer (CT) excitons. This leads to the formation of hydrogen-like ion complexes, CT plaquettes, in the vicinity of the dopant; a CT exciton resonantly interacting with band states can form in these CT plaquettes. The geometry of the arrangement of CT plaquettes in the basal plane of the crystal is determined by its crystalline structure and the type of dopant; therefore, the dopant concentration range corresponding to the existence of a percolation cluster of CT plaquettes can readily be determined for each particular compound. For a number of well-investigated HTSCs (cuprates and pnictides), the indicated concentration ranges are quite consistent with the locations of superconducting domes in the experimental phase diagrams.

The close proximity of doping impurities leads to the emergence of paired plaquette complexes (HL centers)

residing in the basal plane and representing the pairs of adjacent ions of one sign surrounded by ions of the other sign (a solid state analog of the hydrogen molecule). Two electrons and two holes can form a bound biexciton state in this center, owing to the possibility of two holes (in cuprates) or two electrons (in pnictides) in the singlet state being in the space between the central ions and attracted simultaneously to two electrons (holes) on these ions. The existence of such HL centers makes it possible to explain the generation of additional free carriers in the normal state and the emergence of superconducting pairing.

Acknowledgments
The authors are grateful to A A Gorbatsevich for useful discussions and critical comments. The work was supported by the RFBR grant No. 14-02-0078516.

References

1. Varma C M, Schmitt-Rink S, Abrahams E *Solid State Commun.* **88** 847 (1993)
2. Kumagai K et al. *J. Supercond.* **7** 63 (1994)
3. Segawa K, Ando Y *Phys. Rev. Lett.* **86** 4907 (2001)
4. Krockenberger Y et al. *Phys. Rev. B* **77** 060505(R) (2008)
5. Ni N et al. *Phys. Rev. B* **78** 214515 (2008)
6. Kamihara Y et al. *J. Am. Chem. Soc.* **130** 3296 (2008)
7. Oka T et al. *Phys. Rev. Lett.* **108** 047001 (2012)
8. Li Z et al. *Phys. Rev. B* **86** 180501(R) (2012)
9. Sun Y et al. *AIP Adv.* **3** 102120 (2013)
10. Segawa K, Ando Y *Phys. Rev. B* **69** 104521 (2004)
11. Rullier-Albenque F et al. *Phys. Rev. Lett.* **103** 057001 (2009)
12. Fang L et al. *Phys. Rev. B* **80** 140508(R) (2009)
13. Haskel D, Polinger V, Stern E A *AIP Conf. Proc.* **483** 241 (1999)
14. Hammel P C et al. *Phys. Rev. B* **57** R712 (1998)
15. Wadati H, Elfimov I, Sawatzky G A *Phys. Rev. Lett.* **105** 157004 (2010)
16. Berlijn T et al. *Phys. Rev. Lett.* **108** 207003 (2012)
17. Levy G et al. *Phys. Rev. Lett.* **109** 077001 (2012)
18. Singh D J, Du M-H *Phys. Rev. Lett.* **100** 237003 (2008)
19. Singh D J *Phys. Rev. B* **78** 094511 (2008)
20. Sadovskii M V *Phys. Usp.* **51** 1201 (2008); *Usp. Fiz. Nauk* **178** 1243 (2008)
21. Mitsen K V, Ivanenko O M *Phys. Usp.* **47** 493 (2004); *Usp. Fiz. Nauk* **174** 545 (2004)
22. Mitsen K V, Ivanenko O M *Eur. Phys. J. B* **52** 227 (2006)
23. Jacobsen J L *J. Phys. A* **47** 135001 (2014)
24. Poccia N et al. *Appl. Phys. Lett.* **104** 221903 (2014)
25. Poccia N, Lankhorst M, Golubov A A *Physica C* **503** 82 (2014)
26. Takagi H et al. *Phys. Rev. Lett.* **68** 3777 (1992)
27. Mitsen K V, Ivanenko O M *JETP* **107** 984 (2008); *Zh. Eksp. Teor. Fiz.* **134** 1153 (2008)
28. Nagano T et al. *Phys. Rev. B* **48** 9689 (1993)
29. Slater J C *J. Chem. Phys.* **41** 3199 (1964)
30. Uemura Y J *Physica B* **404** 3195 (2009)
31. Kuhler A, Behr G *MRS Proc.* **1254** 1254-L01-04 (2010)
32. Matusiak M, Wolf T *Phys. Rev. B* **92** 214515 (2015)
33. Harshman D R, Mills A P (Jr.) *Phys. Rev. B* **45** 10684 (1992)
34. Eliashberg G M *JETP Lett.* **46** S81 (1987); *Pis'ma Zh. Eksp. Teor. Fiz.* **46** S94 (1987)
35. Kulik I O *Sov. J. Low Temp. Phys.* **13** 505 (1987); *Fiz. Nizk. Temp.* **13** 879 (1987)
36. Mitsen K V, Ivanenko O M *JETP Lett.* **82** 129 (2005); *Pis'ma Zh. Eksp. Teor. Fiz.* **82** 144 (2005)
37. Volkov B A, Tugushev V V *JETP Lett.* **46** 245 (1987); *Pis'ma Zh. Eksp. Teor. Fiz.* **46** 193 (1987)
38. Arseev P I *Sov. Phys. JETP* **74** 667 (1992); *Zh. Eksp. Teor. Fiz.* **101** 1246 (1992)
39. Simanek E *Solid State Commun.* **32** 731 (1979)
40. Ting C S, Talwar D N, Ngai K L *Phys. Rev. Lett.* **45** 1213 (1980)
41. Schüttler H-B, Jarrell M, Scalapino D J *Phys. Rev. Lett.* **58** 1147 (1987)
42. Little W A *Phys. Rev. A* **134** A1416 (1964)
43. Ginzburg V L *Sov. Phys. JETP* **20** 1549 (1965); *Zh. Eksp. Teor. Fiz.* **47** 2318 (1964)